Tag-Based Sensing and Positioning in Passive UHF RFID: Tag Reflection

Daniel Arnitz
Signal Proc. and Speech Comm. Lab
Graz Univ. of Technology, Austria
daniel.arnitz@tugraz.at

Ulrich Muehlmann
NXP Semiconductors
Gratkorn, Austria
ulrich.muehlmann@nxp.com

Klaus Witrisal
Signal Proc. and Speech Comm. Lab
Graz Univ. of Technology, Austria
witrisal@tugraz.at

***Abstract* - We present a comprehensive model of the complex reflection coefficient of UHF RFID tags during modulation. The model is based on an equivalent circuit and validated using measurements of an NXP UCODE G2XM on an NXP UCODE general purpose reference antenna in an anechoic chamber. Using this model, we conduct an analysis of the influence of assembly tolerances and antenna detuning on accuracy in a frequency-domain phase-based ranging approach. The tools used in this analysis are also applicable to tag antenna based sensing and are available under GNU GPL as part of the PARIS simulation framework, a simulation tool intended to serve in the development and testing of backscatter-based sensing and positioning.**

I. Introduction

UHF RFID has come a long way since its early stages in the 1970s and the first standardization in the early 2000s [1]. Since then, it has become ubiquitous in various applications from supply chain management to laundry services. Even though UHF RFID is now a widespread technology, reliable positioning is a feature that is not yet available. There has been considerable research on UHF RFID positioning during the last years, but no conclusive breakthrough [2].

Foremost in the list of reasons for this are the need to keep the tag simple (power consumption, costs) and the strict bandwidth limits of the UHF RFID frequency band(s). As a consequence, the used ranging methods are based on narrowband parameters such as return link phases and thus especially vulnerable to multipath propagation. A comprehensive overview of such phase-based ranging and positioning systems currently under research can be found in [2]. Even though the error for phase-based ranging methods in typical supply chain management applications such as portals is dominated by multipath propagation [2–4], the error caused by tag phase shifts can become significant in light multipath environments. This error depends on the detuning of the tag and is thus a parameter that typically cannot be controlled. Detuning is a major issue in conventional RFID systems [5], but also offers opportunities when it is used for tag-based sensing [6–8].

In Section II we will introduce two models of the tag reflection that will subsequently be used in Section IV to investigate the effects of detuning on a phase-based ranging system [4]. In Section III the used models are validated using reflection coefficient measurements of a Gen-2 tag in situ, i.e, during its normal operation in the electromagnetic field.

II. Tag Modeling

The only physical tag parameter visible to the reader is the tag's reflection coefficient, which makes it the most important tag parameter for backscatter-based sensing and positioning. The reflection coefficient of passive tags is highly frequency dependent, nonlinear, and time-variant.

The presented model uses impedance data of chip (modulated and unmod.), assembly, and antenna to calculate the reflection coefficient of the fully assembled tag. These impedances can be obtained via conducted measurements [9, 10] or simulations, while measuring the reflection coefficient directly requires an anechoic environment [11].

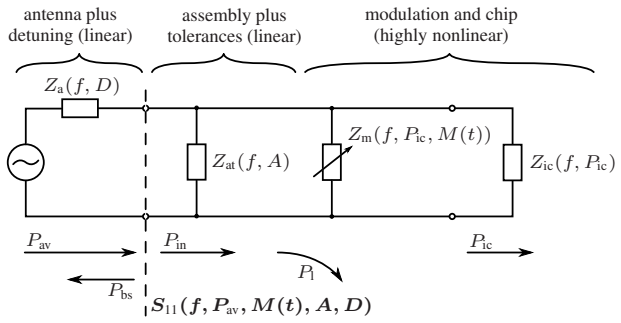

FIGURE 1 - EQUIVALENT CIRCUIT MODEL

2.1 Equivalent Circuit Model

The equivalent circuit model shown in Fig. 1 is applied to keep the complexity manageable. Similar equivalent circuits are well established in RFID [1, 12, 13].

As a first step in the calculation of the tag's reflection coefficient, modulation and chip impedance are combined for different modulation states, forming a three-dimensional matrix (over frequency f, chip power P_ic, and modulation state M).

As a next step the assembly impedance Z_at is computed (parallel RC). This impedance models the mounting of the chip on the antenna (flip-chip, TSSOP plus soldering, ...), including tolerances. The parallel capacity is chosen depending on the assembly tolerance state A, and the Ohmic part is calculated using Q-matching (e.g, [14, 15]) between antenna and load impedance at the intended frequency of operation (typ. 915 MHz) and the tag's power threshold $P_\mathrm{ic,min}$, [10]. This approach reflects the effort of a manufacturer to still match the tag "as well as possible" for a given assembly process. As the assembly is not fully predictable and will also affect the resistance, the optimally tuned resistor is subsequently multiplied by a scalar factor which, like the chosen capacity, depends on the assembly tolerance state A. By using a factor instead of a constant resistance the results stay independent of the actual matching point. Using the assembly impedance Z_at the power losses in modulation impedance and assembly can be calculated, thus making the input power P_in known:

$$P_\mathrm{in} = P_\mathrm{ic} \cdot \left(1 + \frac{R_{\mathrm{at}\|\mathrm{m}} \cdot |Z_\mathrm{ic}|^2}{R_\mathrm{ic} \cdot |Z_{\mathrm{at}\|\mathrm{m}}|^2}\right) \tag{1}$$

The third step takes detuning of the antenna near objects into account. Especially near metal, the antenna self-resonance is considerably boosted. Detuning will also shift this resonance to lower frequencies. A detuning model has been implemented that modifies the antenna impedance in free space by increasing the quality factor and shifting the antenna self-resonance in frequency, as shown in Fig. 2. This heuristic model is based on nonlinear interpolation of the antenna impedance to emulate the effects of close-by water and metal objects. It has been derived from impedance measurements of an NXP UCODE general purpose antenna and is controlled by two

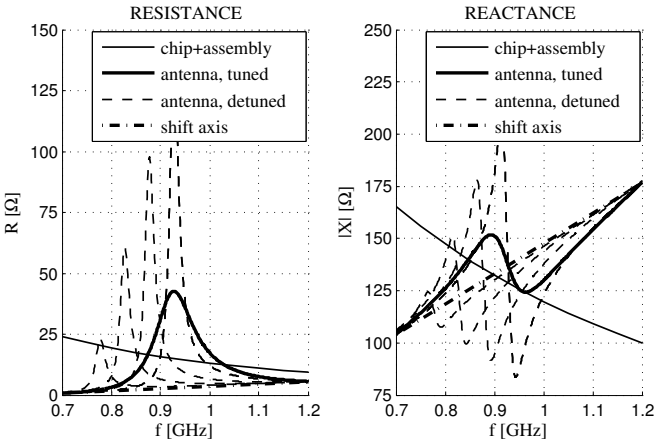

FIGURE 2 - EXAMPLES FOR IMPEDANCES OF CHIP (FLIP-CHIP ASSEMBLY) AND ANTENNA (TUNED AND DETUNED).

parameters: percent enhancement and frequency shift of the antenna self-resonance. The first parameter controls a compression of the frequency axis around the resonance and an expansion of R- and X-axes. The second parameter controls the frequency shift along the shift axis of R_a and X_a, as well as the increasing attenuation of the resonance for large frequency shifts (cf. Fig. 2). The combination of both parameters forms the detuning state D. Note that this method will only give qualitatively correct results. Specifically, it does not consider additional resonances created by close coupling, the alteration and shifting of resonances other than the main antenna self-resonance, the effects of different orientations of the antenna relative to the offending material, or compound materials. However, these limitations only apply to the modeling of detuning, not the entire equivalent circuit model. If high accuracy is required, measured impedances of detuned antennas can easily be used instead.

As a final step, the reflection coefficient (S_{11}) at the connection between antenna and combined tag impedance

$$S_{11} = \frac{Z_\mathrm{a} - Z^*_{\mathrm{at}\|\mathrm{m}\|\mathrm{ic}}}{Z_\mathrm{a} + Z_{\mathrm{at}\|\mathrm{m}\|\mathrm{ic}}} \tag{2}$$

as well as the incident/available power level P_av are computed (* denotes the complex conjugate)

$$P_\mathrm{av} = P_\mathrm{in} / \left(1 - |S_{11}|^2\right). \tag{3}$$

So far, the combined impedances and the reflection coefficient are functions of the chip power P_ic. A more practical dependence would be P_av here, as it is a value that can be directly derived from channel models, thus giving the tag (reflection coefficient) model a well-defined interface. For this reason the reflection coefficient is re-interpolated using the connection between available (incident) and chip power levels $P_\mathrm{av}(f, P_\mathrm{ic}, ...)$, forming the final reflection coefficient over frequency, incident power, modulation, assembly, and detuning $S_{11}(f, P_\mathrm{av}, M, A, D)$. Note that antenna gain pattern and polarization mismatch are not included in this model. This is a very common and useful simplification; they can, however, be factored in at any later time, cf. [16–19].

2.2 Linear Model of the Tag Modulation

This linear model is a simplification of the quite complex reflection coefficient trajectory during modulation, cf. Fig. 3. A more detailed description can be found in [4]. The model replaces the trajectory by a fictive center ρ and a difference $\Delta\rho$, where

$$\text{“mod”} = \rho + \Delta\rho \qquad \text{and} \qquad \text{“unmod”} = \rho - \Delta\rho \tag{4}$$

This approach is loosely linked to differential radar cross sections, cf. [20]. Note that the end points of the trajectory are power and frequency

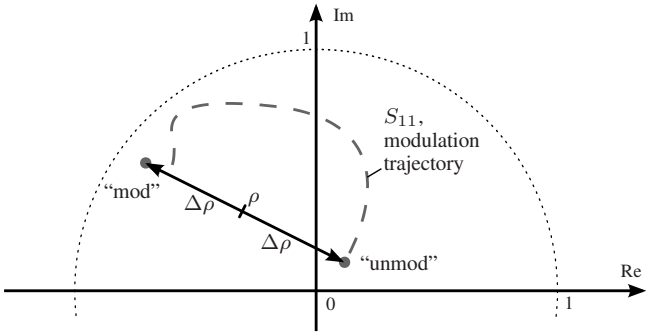

FIGURE 3 - LINEAR MODEL OF THE REFLECTION COEFFICIENT: ONLY THE END POINTS OF THE MODULATION TRAJECTORY ARE PRESERVED.

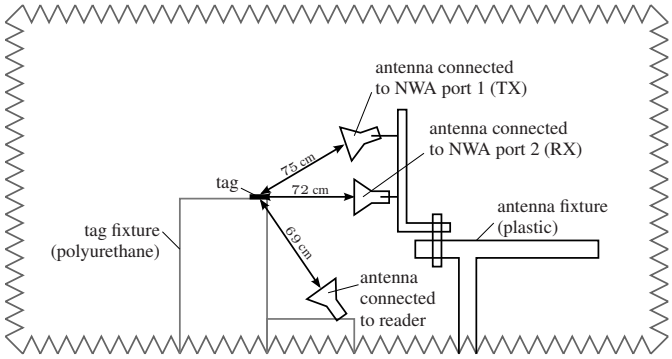

FIGURE 4 - BISTATIC NWA MEASUREMENT SETUP WITH A UHF RFID READER FOR POWER SUPPLY (NOT TO SCALE).

dependent, hence also the parameters of the linear model depend on frequency and power, i.e., $\rho{=}\rho(f, P)$ and $\Delta\rho{=}\Delta\rho(f, P)$.

The benefit of this model is its simplicity when it comes to modulation. The complex reflection coefficient during modulation can be expressed by

$$S_{11}(f, P, t) = \underbrace{\rho(f, P)}_{\text{center}} + \underbrace{s_\mathrm{M}(t)}_{\text{modulation}} \cdot \underbrace{\Delta\rho(f, P)}_{\text{difference}} \tag{5}$$

with $-1{\leq}s_\mathrm{M}(t){\leq}1$. The modulation model in (5) is especially useful for multiple frequency components if the power level is roughly constant and hence the superposition principle holds, cf. [4].

2.3 Underlying Data

The above models are implemented as part of the tag model in the PARIS simulation framework [21, 22], which is available under the GNU General Public License[1]. There are also several predefined lookup tables available with the framework, including the ones we have used in Section IV. Modulation and chip impedance of these tables are based on conducted measurements performed by NXP Semiconductors using the method in [9]. The antenna impedance was calculated using CST and verified using a network analyzer during the validation measurements.

III. MODEL VALIDATION (MEASUREMENTS)

The above models are based on well-established theory and, with the exception of the antenna impedance, on measured data. Nontheless, the calculations leading to the reflection coefficient rely on several simplifications, thus making validation necessary. For this reason we have measured the reflection coefficient of the tag during modulation in an anechoic chamber. In order to also validate the linear model

[1] http://www.gnu.org/licenses/gpl.html

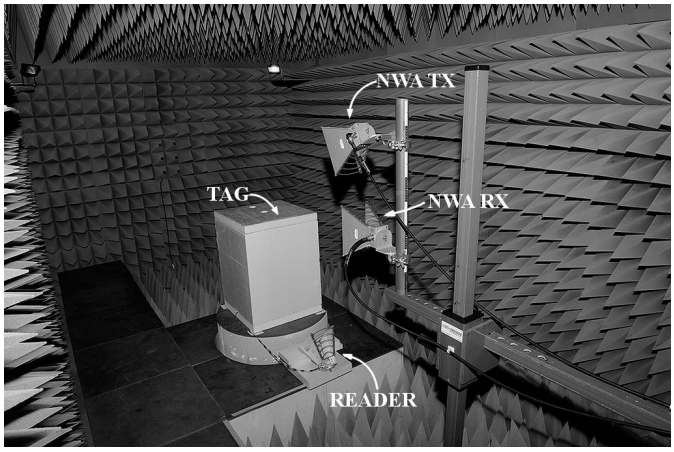

FIGURE 5 - PHOTOGRAPH OF THE ANECHOIC CHAMBER'S INTERIOR WITH THE MEASUREMENT SETUP.

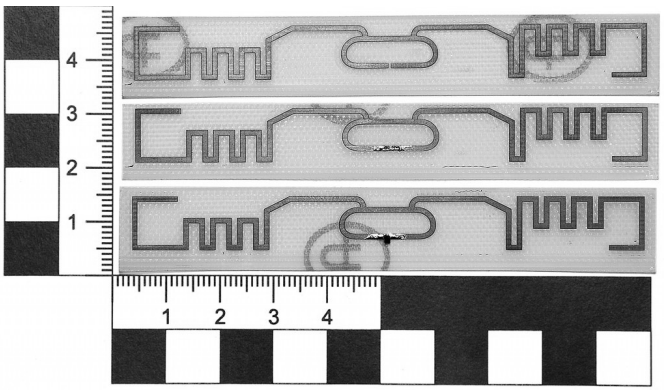

FIGURE 6 - PHOTOGRAPH OF USED CALIBRATION REFERENCES OPEN (TOP) AND SHORT (MIDDLE), AND USED TAG (NXP UCODE G2XM; BOTTOM). SCALE IS IN CM.

of the tag reflection, the calculation of the reflection coefficient from measured data is based on this model.

The used measurement procedure combines several approaches [9, 11, 23] to obtain the complex reflection coefficient of a UHF RFID tag during modulation in the field. To this end, we adapted the procedure in [9], which is a well established procedure for conducted measurements of the chip impedance during modulation: The tag was placed in an anechoic chamber at a short distance from three ETS Lindgren Model 3115 horn antennas (cf. Figs. 4 and 5). The bottom antenna was connected to a Sirit IN510 reader. This reader was used to supply the tag during measurements and to send a custom command setting the tag to continuous modulation at 80 kHz. Middle and uppermost antenna were connected directly to a Rohde&Schwarz ZVA-24 network analyzer (NWA), which was recording S_{21} in a time sweep at an effective sampling frequency of 248.6 kHz. We chose the bistatic setup for its superior isolation compared to directional couplers and circulators. The short distance at the lower end of the far-field ($2D^2/\lambda \approx 73$ cm) minimizes calibration issues.

The major drawbacks of the used method are speed and calibration: Even though the reader carrier is attenuated by the measurement procedure because its period is shorter by factors than the measurement time, changes in the noisefloor are considerable. This makes the recording of several thousand periods of the modulation necessary. Furthermore, the environmental reflections exceed the reflection of the antenna outside its resonance even in an anechoic chamber, making measurements outside its center frequency unreliable.

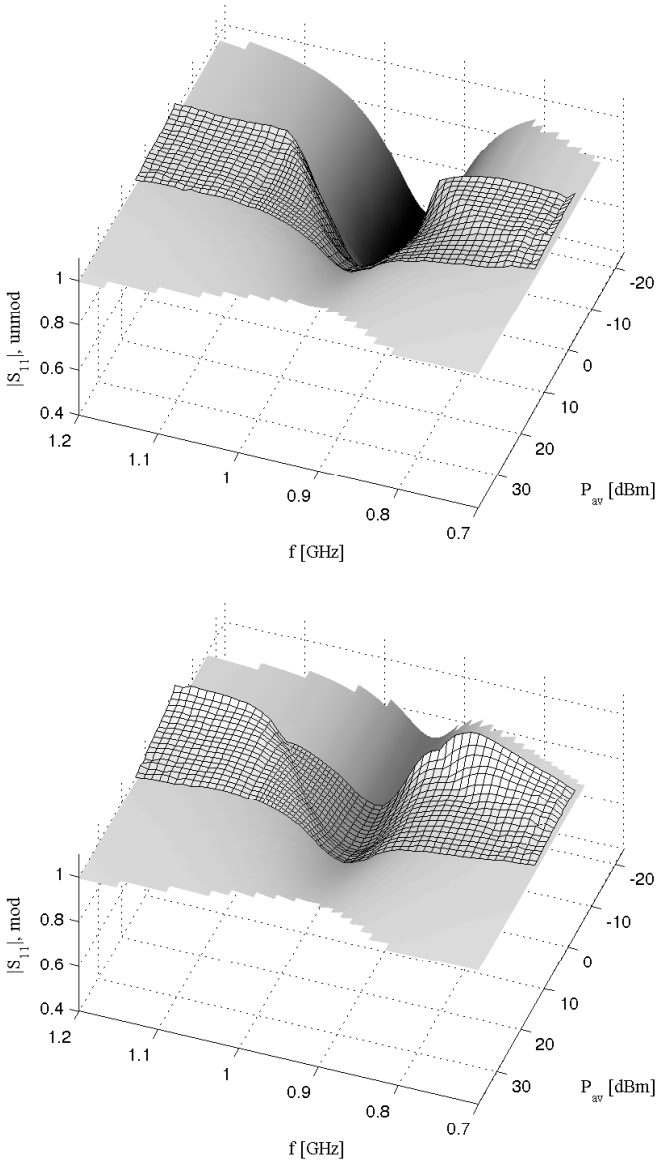

FIGURE 7 - COMPARISON OF UNMODULATED (TOP) AND MODULATED (BOTTOM) REFLECTION COEFFICIENT MAGNITUDES: SIMULATION MODEL VS. MEASUREMENT (GRIDLINES).

Calibration was performed by measuring open- and short-references (Fig. 6). The match reference was produced by measuring the reflection of the empty chamber. Time-sweeps with 10,000 samples were recorded for 59 points between 0.7 GHz and 1.2 GHz and power levels from 13 to 30 dBm in 1 dBm steps at the reader output port. Correction of the measured S_{21} was performed to short $S_{21,s}$ and match $S_{21,m}$ references [23]:

$$S_{11,\text{corr}} = S_{21,\text{corr}} = \frac{S_{21} - S_{21,m}}{S_{21,s} - S_{21,m}} \tag{6}$$

A full calibration, also taking the open-reference into account, was discarded due to numerical instabilities.

The backscatter modulation is subsequently extracted from $S_{11,\text{corr}}$ via the linear model using (4) and (5). A comparison between this measured reflection coefficient and its model can be found in Fig. 7. Note that the measured reflection coefficient slightly exceeds $|S_{11}| = 1$ outside 900−1000 MHz due to the above mentioned calibration problems. Furthermore, we were not able to reconstruct the reflection coefficient phase for the same reason; a full calibration is too instable. The reconstructed magnitude on the other hand is

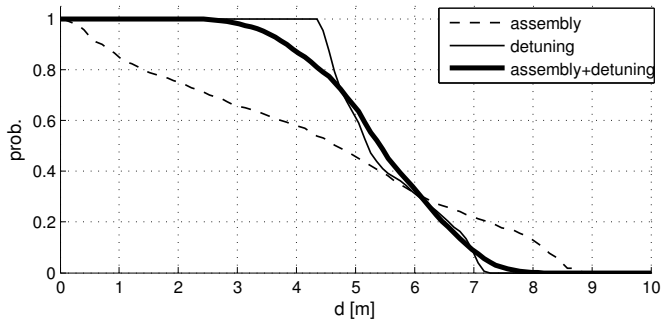

FIGURE 8 - CDFS OF THE MAXIMUM READ RANGE (EU BAND) FOR ALL SCENARIOS.

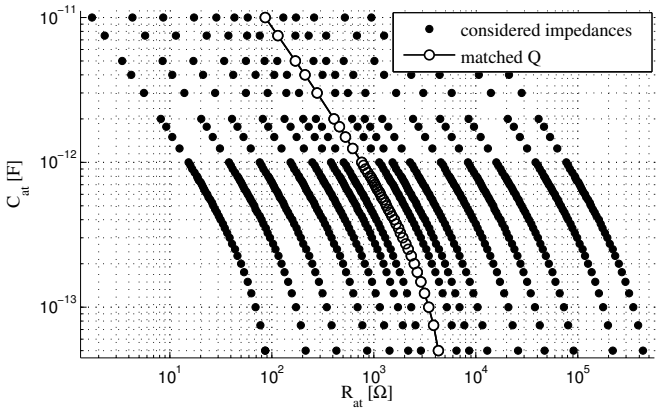

FIGURE 9 - USED ASSEMBLY IMPEDANCES FOR THE ASSEMBLY MISMATCH SIMULATION.

a near-perfect match, with a residual mean absolute error of 0.022 ($|S_{11}|\in[0,1]$). Also the calculated "best fit" assembly, R_{at}=235 Ω parallel to C_{at}=475 fF, corresponds well with soldering the G2XM on milled FR-4.

Hence, in combination with the well established theory of equivalent circuits for antenna systems, this result indicates the validity of the equivalent circuit model and the linear model described above.

IV. IMPACT OF ASSEMBLY TOLERANCES AND DETUNING ON PHASE-BASED RANGING

4.1 Introduction and Used Setup

We have used the above model in a parameter sweep simulation in order to investigate the effects of assembly and detuning on the ranging error of [4], which is a phase-based ranging approach for passive UHF RFID. For the presented investigation we have evaluated three different scenarios: Assembly mismatch (well-matched to complete mismatch), antenna detuning (well-tuned to near-metal), and combined (typical combinations of mismatch and detuning). The chip/antenna combination is again the NXP G2XM on the UCODE general purpose reference antenna. Power levels are varied from 3.28 W EIRP (limit for EU) to the tag minimum power threshold level for all simulations; the reader sensitivity is assumed to be −80 dBm. The employed channel model is a free-space path loss model (pathloss factor 2).

Cumulative distribution functions (CDFs) of the maximum read range in the EU frequency band are given in Fig. 8. The maximum read ranges for well-tuned and well-matched tags approach 10 m, which fits previous findings for this chip ($P_{\text{min}} \approx -13$ dBm) [10]. The maximum read range for detuned tags, on the other hand, is in the range of 3 m (assembly+detuning).

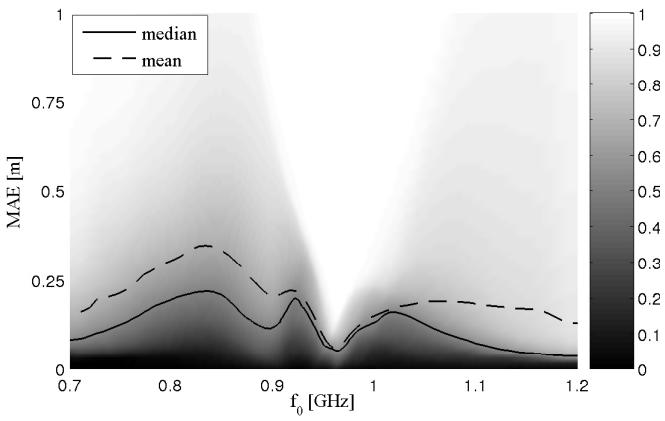

FIGURE 10 - CDF OF THE MEAN ABSOLUTE RANGING ERROR (MAE) FOR A SINGLE CARRIER PAIR OVER FREQUENCY (ALL DISTANCES); ASSEMBLY TOLERANCES.

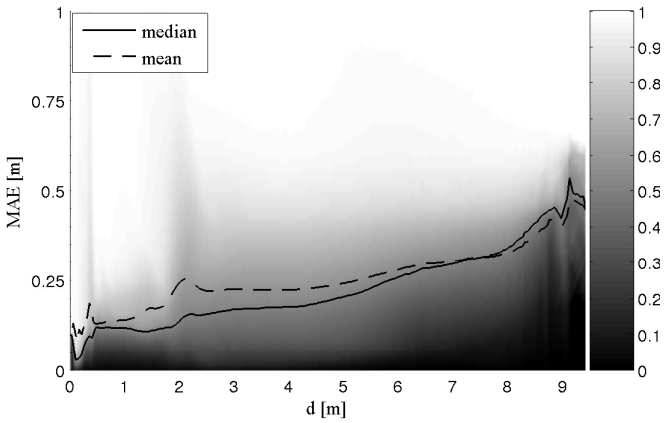

FIGURE 11 - CDF OF THE MEAN ABSOLUTE RANGING ERROR (MAE) OVER DISTANCE FOR ALL UHF RFID FREQUENCIES; ASSEMBLY TOLERANCES.

4.2 Assembly Mismatch

For the presented investigation the assembly capacity has been varied from 50 fF to 10 pF, while the assembly resistance was varied between 2 and 10,000 % of the ideal (Q-matched) value, cf. Fig. 9. This covers perfect assemblies as well as completely messed-up ones.

Fig. 10 shows the cumulative distribution function (CDF) of the mean absolute ranging error (MAE) for one carrier pair (2-frequency continuous wave ranging 2FCW, cf. [4]) with a frequency spacing of Δf=1 MHz at different center frequencies. The error is smallest around 960 MHz, which is the upper turning point of the antenna self-resonance, cf. Fig. 2. At this point the shapes of antenna and chip reactance are similar, thus creating a flat phase that is virtually independent of assembly mismatches. The largest errors are created at transitions between areas where the unmodulated state is better matched to the antenna impedance than the modulated impedance and areas where this matching is reversed. At these crossings the phase of $\Delta\rho$ is subject to fast changes which result in large ranging errors.

A CDF for a carrier placement uniformly distributed over the UHF RFID frequency ranges (865−868 MHz, 902−928 MHz, and 952−954 MHz) can be found in Fig. 11. For high power levels, i.e., short distances, the tag is mismatched by design because the incident power level is considerably higher than the needed chip power. This creates a flat phase and limits the effects of any additional mismatch. With decreasing power, the tag impedance gets closer to the matching

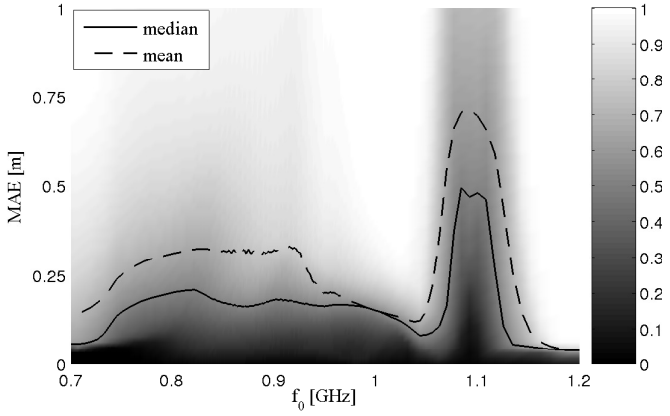

FIGURE 12 - CDF OF THE MEAN ABSOLUTE RANGING ERROR (MAE) FOR A SINGLE CARRIER PAIR OVER FREQUENCY (ALL DISTANCES); ANTENNA DETUNING.

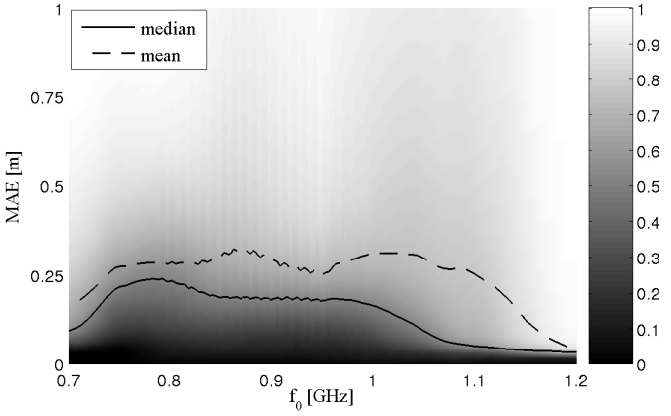

FIGURE 14 - CDF OF THE MEAN ABSOLUTE RANGING ERROR (MAE) FOR A SINGLE CARRIER PAIR OVER FREQUENCY (ALL DISTANCES); COMBINED MISMATCH/DETUNING.

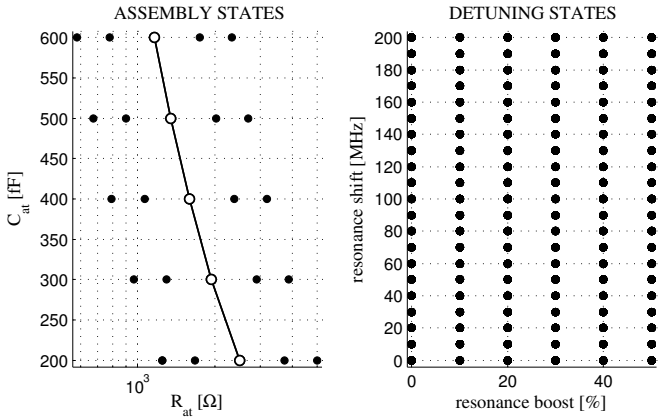

FIGURE 13 - USED ASSEMBLY / DETUNING STATES FOR THE COMBINED MISMATCH SIMULATION.

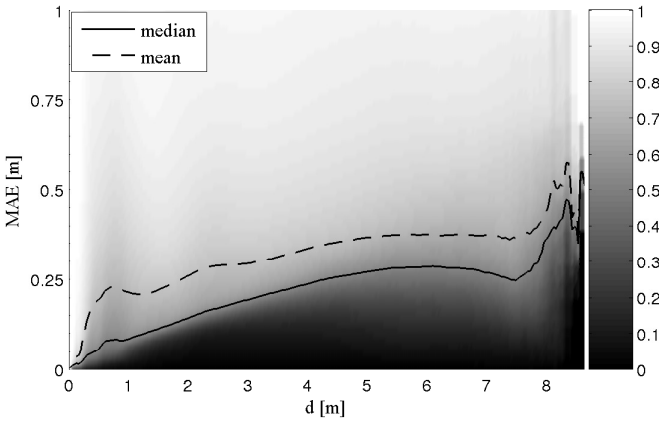

FIGURE 15 - CDF OF THE MEAN ABSOLUTE RANGING ERROR (MAE) OVER DISTANCE FOR ALL UHF RFID FREQUENCIES; COMBINED MISMATCH/DETUNING.

point, increasing the quality factor of the entire system, i.e., making it more resonant. For this reason, the error increases for higher distances.

4.3 Antenna Detuning

For this study we have boosted the resonance of a perfectly matched tag (flip-chip assembly) between $-30\,\%$ (slightly weaker resonance) up to $100\,\%$ (near-metal). The frequency of the resonance was reduced by up to 200 MHz in 5 MHz steps. This selection of parameters corresponds to tags in free space as well as tags that are separated from metal by roughly one centimeter (e.g., two sheets of corrugated fiberboard). Tags directly on metal are not covered by this simulation.

Fig. 12 shows the MAE over frequency for antenna detuning. The errors below 1 GHz are caused by the boosted resonance leading to steeper gradients in the tag's phase. This error decreases for massive detuning, as the resonance is shifted towards lower frequencies and attenuated in magnitude. The error around 1.1 GHz is caused by near-zero modulation depth. Just like for the assembly mismatch, areas with near-zero modulation depth cause steep gradients in the modulation phase and thus large errors.

4.4 Combined Assembly Mismatch / Antenna Detuning

The values chosen here are meant to represent the bulk of used tags. Assembly capacities are varied from 200 fF to 600 fF, the assembly resistance is varied from 50 to $100\,\%$ of the Q-matched value. These assembly impedances cover good to medium flip-chip assemblies. The antenna self-resonance is varied from 100 to $150\,\%$ of its original shape and shifted by up to 200 MHz in 10 MHz steps. The maximum detuning corresponds to tags that are in the vicinity of water. A summary of assembly and detuning states can be found in Fig. 13.

Fig. 14 shows the frequency dependence of the ranging error for this scenario. The combination of detuning and mild assembly tolerances generates an almost uniformly distributed MAE over frequency, with the exception of the frequency range above the antenna self-resonance, where errors are considerably smaller. Even though the average MAE also does not exceed 0.5 m for the chosen mismatch/detuning states in the UHF RFID frequency bands, the peak errors are well above one meter.

The same is true for the errors over distance: While averages (mean and median) do not exceed 0.5 m, the error bound is again in the meter range. The error increases with distance up to the point where heavily detuned and mismatched tags fail. At extreme distances the error is dominated by a relatively small group of well-matched but detuned tags with increased quality factor and small frequency shifts.

V. CONCLUSION

We have presented a simulation model of the complex reflection coefficient of a UHF RFID tag based on its equivalent circuit, as well as a simple linear model that can be used in derivations to describe the tag modulation. Both models have been verified using time-variant reflection coefficient measurements of an NXP UCODE G2XM Gen2 chip

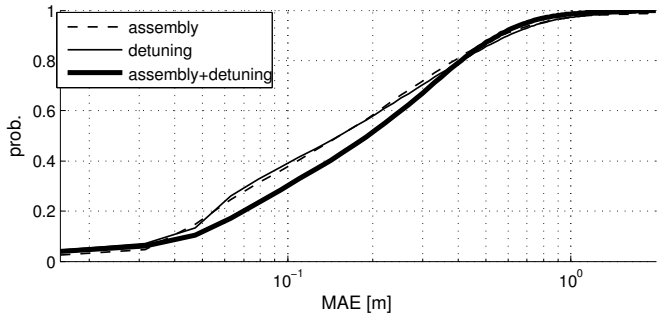

FIGURE 16 - CDFS OF THE MEAN ABSOLUTE RANGING ERROR (MAE) IN THE UHF RFID FREQUENCY BANDS FOR ALL SCENARIOS.

on an NXP UCODE general purpose reference antenna.

Using these models, we have investigated the influence of assembly tolerances and tag detuning on a frequency-domain phase-based ranging system. Although the average mean absolute error (MAE) for this system is below 50 cm, the maximum error may exceed 2 m. A summary CDF for all MAE distance errors in the UHF RFID frequency bands can be found in Fig. 16. Differences between errors caused by assembly mismatches, detuning, or combined mismatch/detuning are minimal.

The reduction in read range due to detuning found in experiments [5] was slightly more pronounced than in the presented simulations. A comparison suggests that the used detuning model is valid if the tag is separated from water/metal by at least 1 cm.

Although the underlying methods and databases [21] have originally been developed to support research on ranging and positioning systems, we hope that they also prove useful for other applications, such as tag-based sensing [6–8].

VI. ACKNOWLEDGMENTS

The authors would like to thank NXP Semiconductors, Gratkorn, Austria, for funding this project and for providing the environment for all measurements. We would also like to thank Giuliano Manzi and Martin Rampetsreiter for their help with the tag models and the measurement setup. This work was supported by the Austrian Research Promotion Agency (FFG) under the grant number 818072.

REFERENCES

[1] D. M. Dobkin, *The RF in RFID*. Elsevier, 2007, ISBN-13: 978-07506820 91.

[2] P. V. Nikitin, R. Martinez, S. Ramamurthy, H. Leland, G. Spiess, and K. V. S. Rao, "Phase based spatial identification of UHF RFID tags," in *Proc. IEEE Int RFID Conf*, 2010, pp. 102–109.

[3] D. Arnitz, G. Adamiuk, U. Muehlmann, and K. Witrisal, "UWB channel sounding for ranging and positioning in passive UHF RFID," in *11th COST2100 MCM*, Aalborg, Denmark, Jun. 2010.

[4] D. Arnitz, K. Witrisal, and U. Muehlmann, "Multi-frequency continuous-wave radar approach to ranging in passive UHF RFID," *IEEE Trans. Microw. Theory Tech.*, vol. 57, no. 5, pp. 1398–1405, Jul. 2009.

[5] S. R. Aroor and D. D. Deavours, "Evaluation of the state of passive UHF RFID: An experimental approach," *IEEE Systems Journal*, vol. 1, no. 2, pp. 168–176, 2007.

[6] R. Bhattacharyya, C. Floerkemeier, and S. Sarma, "RFID tag antenna based temperature sensing," in *Proc. IEEE Int RFID Conf*, 2010, pp. 8–15.

[7] ——, "RFID tag antenna based sensing: Does your beverage glass need a refill?" in *Proc. IEEE Int RFID Conf*, 2010, pp. 126–133.

[8] ——, "Towards tag antenna based sensing - an RFID displacement sensor," in *Proc. IEEE Int RFID Conf*, 2009, pp. 95–102.

[9] L. W. Mayer and A. L. Scholz, "Sensitivity and impedance measurements on UHF RFID transponder chips," in *Int EURASIP Workshop on RFID Techn., Vienna, Austria*, 2007. [Online]. Available: http://publik.tuwien.ac.at/files/PubDat_165917.pdf

[10] P. V. Nikitin, K. V. S. Rao, R. Martinez, and S. F. Lam, "Sensitivity and impedance measurements of UHF RFID chips," *IEEE Trans. Microw. Theory Tech.*, vol. 57, no. 5, pp. 1297–1302, 2009.

[11] P. V. Nikitin and K. V. S. Rao, "Theory and measurement of backscattering from RFID tags," *IEEE Antennas Propag. Mag.*, vol. 48, no. 6, pp. 212–218, 2006.

[12] K. Finkenzeller, *RFID Handbook: Fundamentals and Applications in Contactless Smart Cards and Identification*, 2nd ed. Wiley & Sons, 2003, ISBN-13: 978-0470844021.

[13] E. Colin, A. Moretto, C. Ripoll, and S. A. Chakra, "Delta RCS of UHF RFID taking into account the shunt resistance in the tag model," in *Proc. Joint IEEE North-East Workshop Circuits and Systems and TAISA Conf. NEWCAS-TAISA '09*, 2009, pp. 1–4.

[14] J.-W. Lee, H. Kwon, and B. Lee, "Design consideration of UHF RFID tag for increased reading range," in *Proc. IEEE MTT-S Int. Microwave Symp. Digest*, 2006, pp. 1588–1591.

[15] K. V. S. Rao, P. V. Nikitin, and S. F. Lam, "Impedance matching concepts in RFID transponder design," in *Proc. Fourth IEEE Workshop Automatic Identification Advanced Technologies*, 2005, pp. 39–42.

[16] ——, "Antenna design for UHF RFID tags: a review and a practical application," *IEEE Trans. Antennas Propag.*, vol. 53, no. 12, pp. 3870–3876, 2005.

[17] Y. Tikhov, "Comments on antenna design for UHF RFID tags: a review and a practical application," *IEEE Trans. Antennas Propag.*, vol. 54, no. 6, 2006.

[18] P. V. Nikitin and K. V. S. Rao, "Reply to comments on antenna design for UHF RFID tags: A review and a practical application," *IEEE Trans. Antennas Propag.*, vol. 54, no. 6, pp. 1906–1907, 2006.

[19] W. Wiesbeck, G. Adamiuk, and C. Sturm, "Basic properties and design principles of UWB antennas," *Proc. IEEE*, vol. 97, no. 2, pp. 372–385, 2009.

[20] P. V. Nikitin, K. V. S. Rao, and R. D. Martinez, "Differential RCS of RFID tag," *Electronics Letters*, vol. 43, no. 8, pp. 431–432, 2007.

[21] The PARIS Simulation Framework. Graz University of Technology / NXP Semiconductors. Open-Source (GNU GPL v3). [Online]. Available: http://www.spsc.tugraz.at/research-topics/wireless-communications/paris-osf/

[22] D. Arnitz, U. Muehlmann, T. Gigl, and K. Witrisal, "Wideband system-level simulator for passive UHF RFID," in *Proc. IEEE Intl. Conf. on RFID, RFID'09*, Orlando, Florida, Apr. 2009.

[23] S. Hu, C. L. Law, and W. Dou, "Measurements of UWB antennas backscattering characteristics for RFID systems," in *Proc. IEEE Int. Conf. Ultra-Wideband ICUWB 2007*, 2007, pp. 94–99.